HEAT-BUDGET MEASUREMENTS ON THE QUELCCAYA ICE CAP, PERUVIAN ANDES*

By Stefan Hastenrath

(Department of Meteorology, University of Wisconsin, Madison, Wisconsin 53706, U.S.A.)

Abstract. During the June–August 1976 Quelccaya ice cap expedition, global, SW↓, and net long-wave radiation, LW↑↓, were measured through several complete day–night cycles, and for a wide range of cloudiness conditions. Field work further included albedo measurements along representative transects across the ice cap and lysimeter-type estimates of ablation. Automatic stations recording wind, temperature and sunshine duration were also installed.

Daily totals of SW↓ and LW↑↓ representative of completely clear and overcast days are derived. On this basis, empirical relationships allow the computation of monthly totals of radiation fluxes for an entire year from records of sunshine duration and temperature expected from the automatic stations.

The larger part of the plateau is situated above 5 400 m and has an albedo mostly in excess of 80%. Sub-freezing temperatures essentially limit ablation to the energetically expensive sublimation. For clear sky, daily totals of SW↓ and LW↑↓ are of the order of 312 and 53 W m^{-2}, respectively. With the albedo found, net short-wave radiation SW↑↓ becomes of the same general magnitude as LW↑↓, and the energy left for ablation is near to nil. Cloudiness would reduce both SW↑↓ and LW↑↓, thus largely compensating the effect on the residual net radiation, SWLW↑↓. This is consistent with ablation measurements. Over the larger area of the ice plateau, ablation may be close to zero in a first approximation; some ablation, including melting, takes place near the lower-lying rim of the ice cap, and calving off steep cliffs seems to provide a major mechanism for the disposal of the ice mass.

Résumé. *Mesure de bilan thermique de la calotte glaciaire de Quelccaya dans les Andes Péruviennes.* Au cours de l'expédition de juin–août 1976 à la calotte de Quelccaya, la radiation globale, rayonnement incident de courte longueur d'onde et bilan net des rayonnements incidents et émis en grandes longueurs d'onde, ont fait l'objet de mesures au cours de plusieurs cycles jour–nuit complets pour une gamme étendue de conditions de nébulosité. Les observations courantes ultérieures comprenaient des mesures d'albédo le long de sections transversales de la calotte et des estimations de l'ablation au lysimètre. On a également installé des stations automatiques de mesure du vent, de la température et de la durée d'insolation.

On en a déduit des bilans journaliers des rayonnements incidents et du rayonnement de grande longueur d'onde émis et reçu pour les cas de journées entièrement claires ou totalement couvertes par les nuages. Sur cette base, des relations empiriques permettent le calcul des totaux mensuels du flux radiatif pour une année entière à partir des enregistrements des durées d'ensoleillement et des températures tirées des stations automatiques.

La plus grande partie du plateau est située au-dessus de 5 400 m et a un albédo le plus souvent supérieur à 80%. Une température essentiellement négative limite l'ablation à la seule sublimation très coûteuse en énergie. Pour un ciel clair, les totaux journaliers de rayonnement solaire incident et du bilan de rayonnement de grande longueur d'onde sont de l'ordre respectivement de 312 et de 53 W m^{-2}. Avec l'albédo trouvé, le bilan du rayonnement solaire incident devient du même ordre de grandeur que celui du rayonnement de grande longueur d'onde et l'énergie disponible pour l'ablation est voisine de zéro. La nébulosité réduit à la fois les rayonnements de courte longueur d'onde et de grande longueur d'onde, ce qui équilibre approximativement son effet sur le bilan net résiduel toutes longueurs d'onde. Ces résultats sont cohérents avec les mesures d'ablation. Sur de plus grandes surfaces du plateau glaciaire, l'ablation peut être à peu près nulle en première approximation; une certaine ablation, comprenant de la fusion, intervient près de la limite inférieure de la calotte; et le vêlage de falaises abruptes de glace semble être le mécanisme majeur de la disparition de la masse de glace.

Zusammenfassung. *Wärmehaushaltsmessungen am Quelccaya Eiskap, Peruanische Anden.* Während der Quelccaya-Eiskap-Expedition im Juni–August 1976 wurden die Globalstrahlung, SW↓, und die langwellige Netto-Strahlung, LW↑↓, fortlaufend über mehrere vollständige Tag–Nacht-Zyklen gemessen, und zwar unter unterschiedlichen Bewölkungsverhältnissen. Ferner wurden Albedomessungen längs ausgewählter Profile über das Eisplateau sowie Ablationsmessungen mittels Lysimeter durchgeführt. Ausserdem wurden automatisch Wind, Temperatur, und Sonnenscheindauer registrierende Stationen aufgestellt.

Es werden für völlig wolkenlose und völlig bedeckte Tage repräsentative Tagessummen von SW↓ und LW↑↓ abgeleitet. Auf dieser Grundlage lassen sich Monatssummen der Strahlungsflüsse für ein ganzes Jahr aus den erwarteten automatischen Registrierungen von Sonnenscheindauer und Temperatur mittels empirischer Beziehungen ableiten.

Der grössere Teil des Eisplateaus liegt oberhalb 5 400 m und hat eine Albedo von mehr als 80%. Temperaturen unter dem Gefrierpunkt beschränken die Ablation im wesentlichen auf die energetisch aufwendige Verdunstung. Für wolkenlose Tage repräsentative Tagessummen von SW↓ und LW↑↓ betragen 312 und 53 W m^{-2}. Die kurzwellige Netto-Strahlung hat die gleiche Grössenordnung wie LW↑↓, und die für die

Ablation verbleibende Energie ist nahezu Null. Bewölkung vermindert zugleich SW↓ und LW↑↓ und gleicht somit die Wirkung auf die verbleibende Strahlungsbilanz weitgehend aus. Das stimmt mit den Ablationsmessungen überein. Für den grösseren Flächenanteil des Eisplateaus mag die Ablation in erster Näherung Null sein; mässige Ablation, auch durch Schmelzung findet in den niedriger liegenden Rand-bereichen der Eiskappe statt; indessen scheint das Kalben über steile Klippen einen Hauptmechanismus für den Abtransport der Eismassen darzustellen.

INTRODUCTION

An attempt is being made to reconstruct, for the first time, a tropical climatic record on the basis of isotope and microparticle analysis of ice cores. The Quelccaya ice cap (Figs 1 and 2, and Table I; approximate coordinates lat. 13° 56′ S., long. 70° 50′ W.) appears to offer a unique potential for this purpose because of its high elevation and gentle topography (Mercer and others, 1975). This ice cap in the Andes of south-eastern Peru is part of the easternmost glaciated mountain chain near the drop-off to the wet Amazon basin. Observations
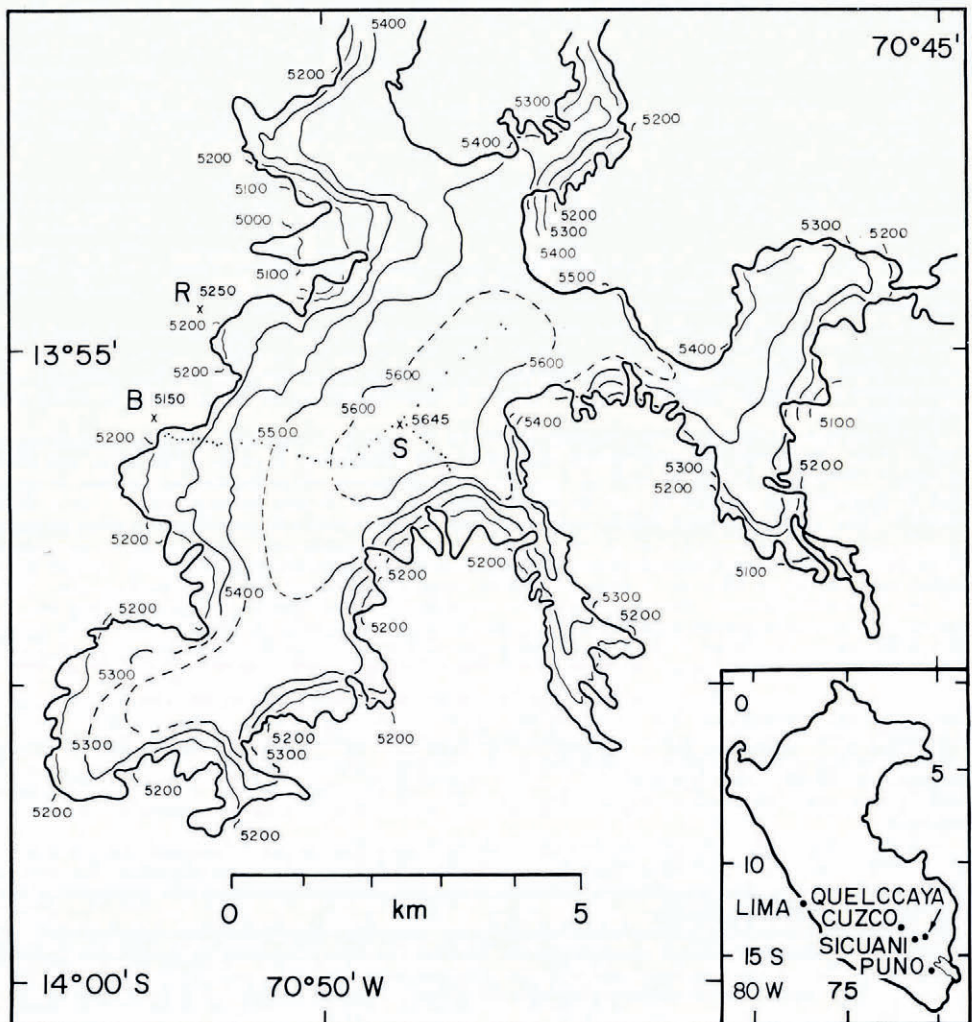

Fig. 1. *Orientation map. S summit, B base camp, elevations in m; ice rim indicated by heavy solid line and albedo traverses by dots. Automatic stations are installed at S and R.*
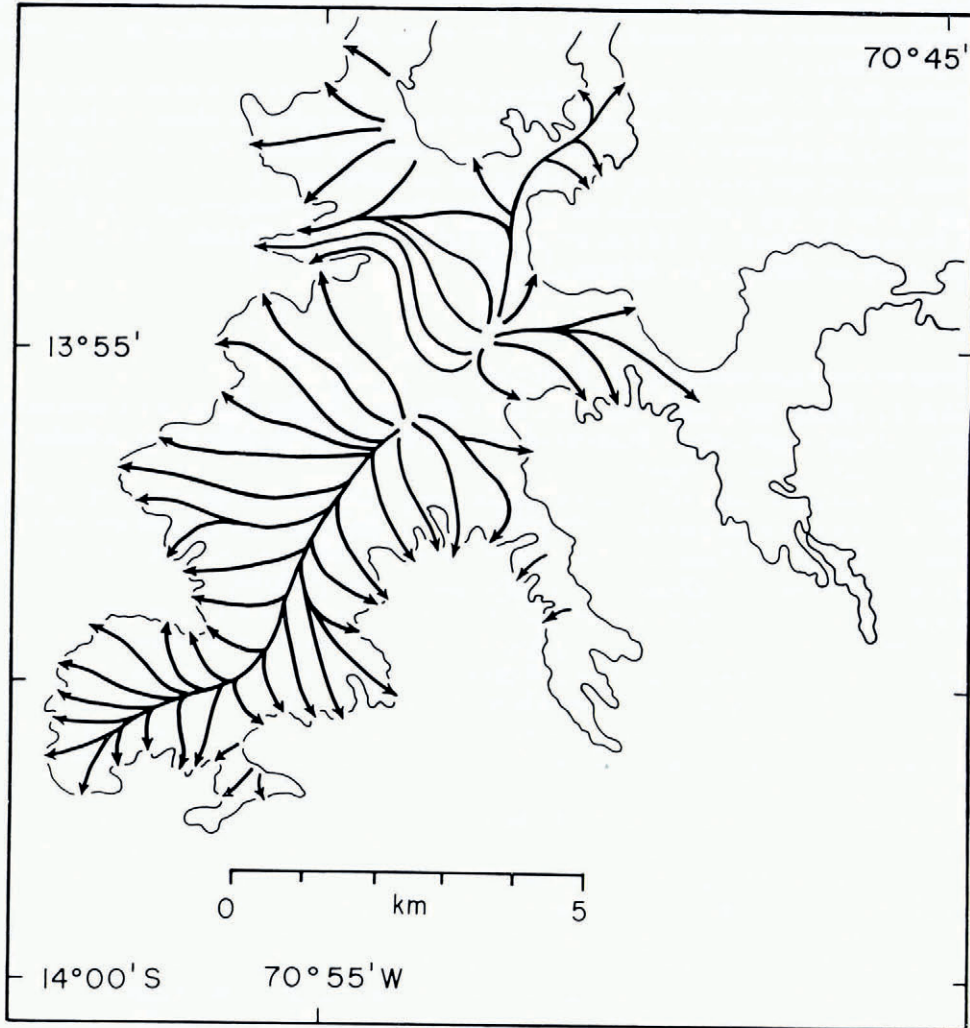
Fig. 2. Approximate flow-line pattern constructed from surface topography.

TABLE I. APPROXIMATE AREA OF QUELCCAYA
ICE CAP BY 100 m ELEVATION INTERVALS AND
REPRESENTATIVE ALBEDO

Elevation m	Area 10^5 m^2	Albedo %
> 5 600	46	80–95
5 600–5 500	92	⩾75
5 500–5 400	152	
5 400–5 300	110	⩾70
5 300–5 200	88	
5 200–5 100	48	40–95
5 100–5 000	4	
5 000–4 900	1	
Total	541	

of the modern meteorological conditions and measurements related to the mass and heat budget are important components of this project conducted by the Institute of Polar Studies, Ohio State University.

During the June–August 1976 expedition, pits were dug and ice samples taken at three locations on the ice cap; accumulation/ablation stakes were laid out along several transects and surveyed tacheometrically; automatic stations recording temperature, wind and sunshine duration, and ideally functioning unattended for an entire year, have been installed on the summit of the ice cap and outside the ice, respectively; and radiation measurements were made for several days on the ice cap and at the ice rim. Only preliminary results of the heat-budget study are discussed in the present paper.

INSTRUMENTATION AND MEASUREMENT PROGRAM

Global radiation $SW\downarrow$ was measured with a Kipp and Zonen pyranometer installed with the conventional white collar. Since we are mostly interested in daily totals, angular errors at low sun angles are not important.

For net radiation $SWLW\uparrow\downarrow$ a home-made design mounted on an arm and levelled by bubble was used. Measurements of $SWLW\uparrow\downarrow$ during day-time are not consistently reliable because of angular and thermal errors related to solar radiation. At night the instrument measures net long-wave radiation $LW\uparrow\downarrow$ only, and performs reliably.

Values from the pyranometer and net radiometer were read on appropriately scaled millivoltmeters, manually recorded, and later converted to energy equivalents. Watches were set daily by radio for exact time check. Measurements with the pyranometer and net radiometer were made in local time, at intervals of 15, 30, or 60 min, as far as other project tasks permitted. The objective was to cover several complete day–night cycles under differing conditions of cloudiness. The installation of these instruments at base camp and summit is shown in Figures 3 and 4.

Concurrent with readings of the pyranometer and net radiometer at the base camp, measurements of temperature and humidity of the air were made using a ventilated Assmann-type psychrometer, and surface temperature was measured with an electrical thermometer. At the summit, temperature was measured with a mercury thermometer.

Surface albedo was measured repeatedly along representative transects using a home-made design. This consists of a commercially available solar cell fitted at the end of a collapsible rod, which is further provided with two bubbles on opposite sides for levelling. The output from the solar cell is read on a meter. Readings are taken in rapid succession, with the solar cell alternately facing upward and downward. Albedo is obtained as a ratio of these values. Accordingly, the solar cell is not calibrated. Angular errors preclude use of this instrument for low sun angles and strongly sloping surfaces. During most of the day and over large areas, however, effective sampling of surface albedo is possible. While $SW\downarrow$ is horizontally relatively uniform, large-scale sampling of albedo rather than monitoring of $SW\uparrow$ at a fixed location seemed most appropriate.

Measurements with pyranometer, net radiometer, and albedometer allow, in principle, an estimate of net long-wave radiation $LW\uparrow\downarrow$, as well as upward, $SW\uparrow$, and downward, $SW\downarrow$, directed short-wave radiation. Downward radiative fluxes provide a heat gain to the ice and are counted positive.

To obtain an estimate of ablation, three white circular plastic bowls of 165 cm² cross-sectional area were used as lysimeters. The bowls were filled to the rim with snow and placed so that their rims stayed at the level of the surrounding undisturbed snow surface. The bowls were weighed several times daily and checked for liquid water. Figure 5 is a photograph of these "poor man's lysimeters".
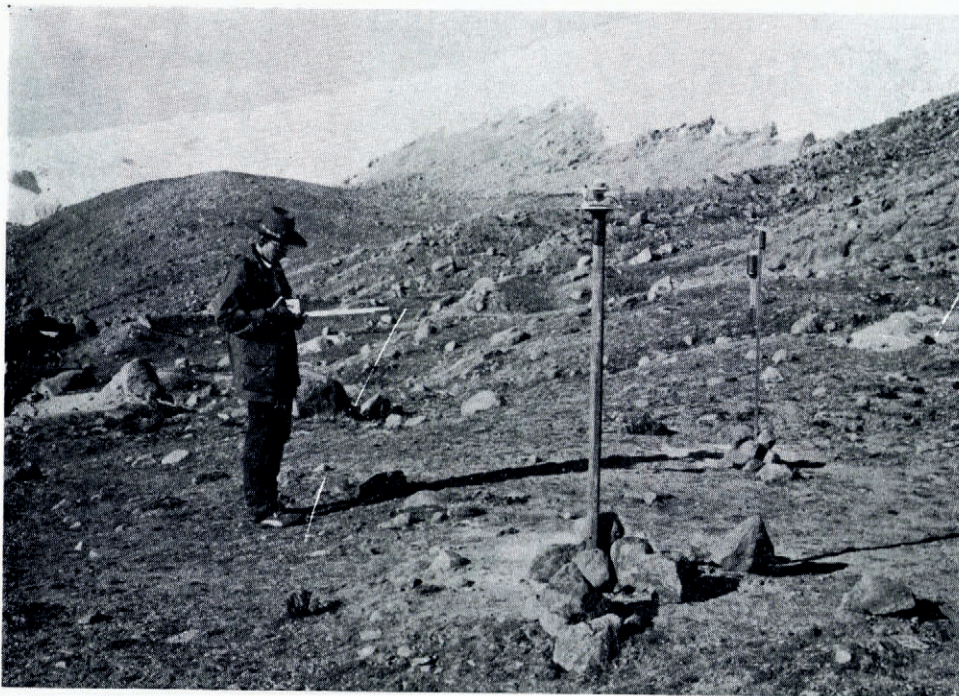
Fig. 3. Kipp and Zonen pyranometer, net radiometer and Assmann psychrometer at base-camp site. (Photograph by S. Hastenrath, June 1976.)
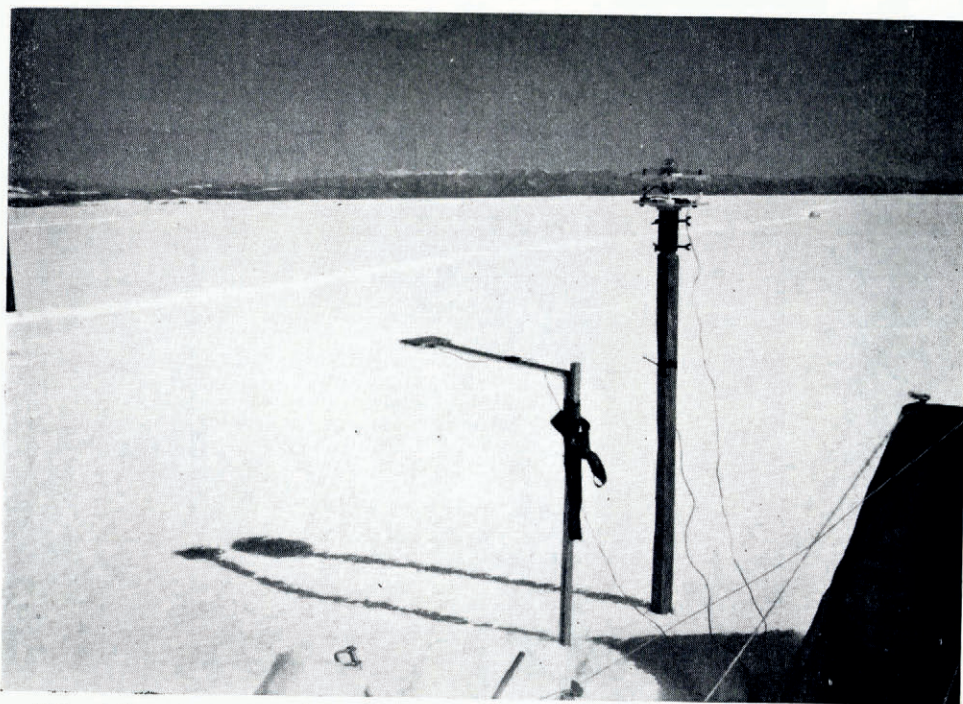
Fig. 4. Kipp and Zonen pyranometer and net radiometer installed at summit site. (Photograph by S. Hastenrath, July 1976.)
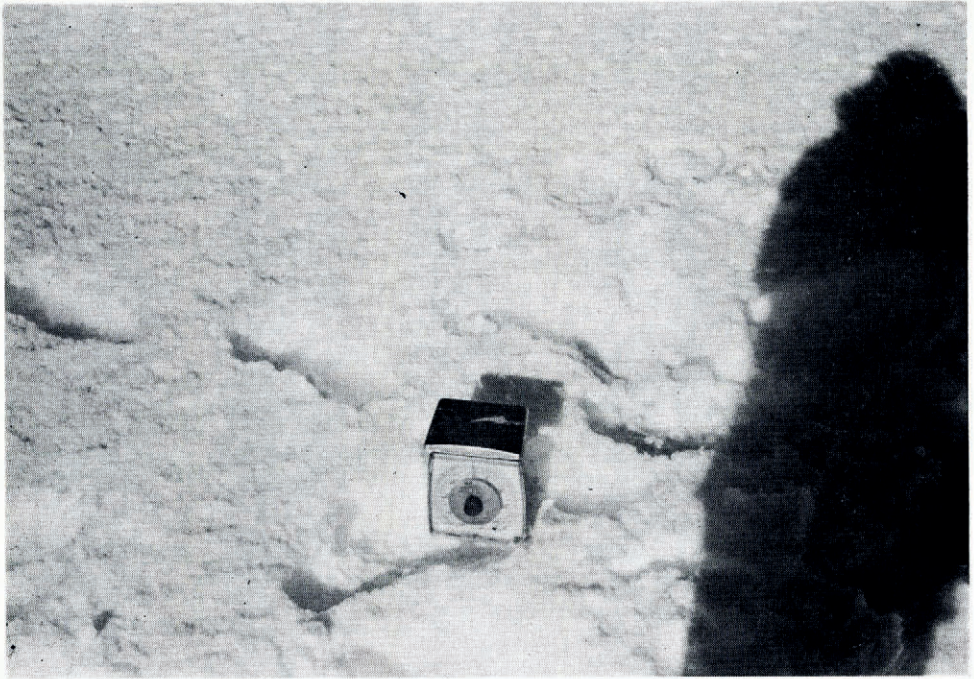
Fig. 5. *Lysimeter bowls and scale at summit site.* (Photograph by S. Hastenrath, July 1976.)

BASE CAMP

The base-camp installation was at 5 150 m near the ice rim (Figs 1 and 3). Radiation measurements were performed continuously from the afternoon of 28 June to the morning of 1 July, and from the evening of 10 July to the evening of 11 July. Sky cover was observed concurrent with the radiation measurements. Sampling ranged from completely clear to overcast.
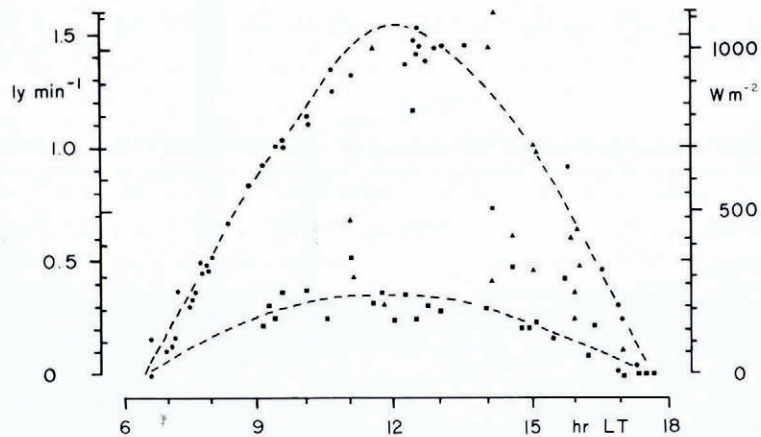

Fig. 6. *Global radiation at base-camp site. Dots, triangles, and squares denote clear sky, fractional cloudiness, and overcast, respectively. Broken lines indicate smoothed daily running means for clear sky and overcast.*

Measurements of SW↓ during all days together are plotted according to local time in Figure 6, with symbols distinguishing between the three categories completely clear, overcast and all other fractions of cloud cover. Broken lines were fitted by hand to indicate the smoothed diurnal running means representative of completely clear and overcast sky, respectively. Daily totals corresponding to these lines, along with the ratio of SW↓ at overcast to that at completely clear sky, are listed in Table II. An estimate of the daily total averaged for 29 and 30 June, and 11 July, is also included for comparison.

TABLE II. RADIATION BUDGET AT QUELCCAYA ICE CAP

	Declination	Summit $+22°\ 28'$		Base camp $+23°\ 17'$	
		SW↓	LW↑↓	SW↓	LW↑↓
		Daily totals W m^{-2}		Daily totals W m^{-2}	
Clear		+312	−52	+304	−54
Overcast		+107	−21	+76	−11
Top of atmosphere		+316		+312	
All days		+244	−51	+201	−40
		Ratios		Ratios	
Overcast / Clear		0.33	0.40	0.25	0.26
Clear / Top of atmosphere		0.987		0.965	
Albedo		0.80		0.20	

Obstruction of the horizon by orographic obstacles was measured by theodolite over all azimuth angles. As is seen from Figure 7, the surrounding topography does not substantially affect the local sunrise/sunset and daily radiation totals. Obstacles are even less important for high sun angles. Figure 6 suggests a tendency for the largest global radiation to occur distinctly after rather than around local noon. Figures 7 and 1 illustrate that at these azimuths sun, station, and the adjacent ice surface would come to lie in one vertical plane. In view of
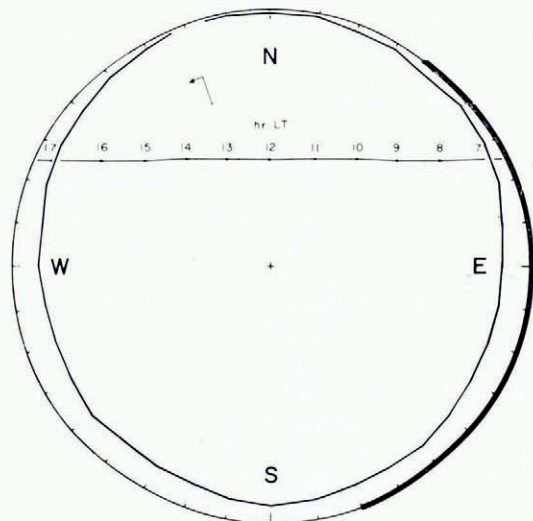

Fig. 7. Angular elevation of local horizon and of sun by azimuth at base-camp site; heavy signature identifies the azimuths with ice surfaces.

the high ice albedo, it is surmised that reflection from the extended white surface leads to the slight asymmetry of the daily radiation curve at the base-camp location. A related effect of reflection from extended ice surfaces on global radiation has been noted by Untersteiner (1957).

Measurements of LW↑↓ during all nights together are plotted in Figure 8 regardless of the hour of night, but distinguishing between completely clear, overcast and with a crude assignment of intermediate cloud cover. A straight line fitted by hand through the point scatter indicates an inverse relation between net long-wave radiation and cloudiness. Values estimated from Figure 8 for completely clear and overcast sky along with their ratio are also listed in Table II. Estimates obtained as averages from the nights following 28, 29, and 30 June, and the night preceding 11 July, are also given for comparison.

Characteristic surface albedo near the base camp, outside the ice, is around 20%. This figure allows the approximate break-down of radiative flux components in Table II.
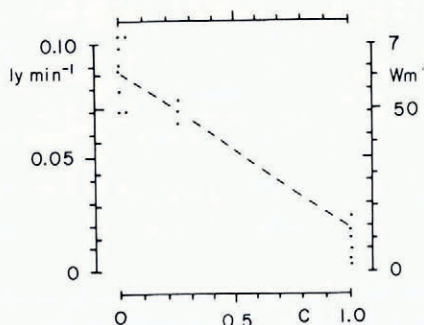

Fig. 8. *Night-time net long-wave radiation* LW↑↓ *at base-camp site with various cloud cover C.*

Summit

A topographic map at a scale of 1 : 25 000 contours all but the highest parts of the ice cap (Peru. Ministerio de Agricultura. Oficina de Catastro Rural, 1976). Tacheometric traverses linking up with reference points of known elevation outside the ice cap completed the topography for the highest areas (Fig. 1). The summit elevation of 5 650 m obtained from traverses with paired Thommen aneroid altimeters compares well with the tacheometric value of 5 645 m.

Radiation measurements at the summit were carried out continuously from around noon of 7 July to the afternoon of 10 July. Sky cover observed concurrent with the radiation measurements ranged from completely clear to overcast.

For the summit site, the horizon was also surveyed by theodolite over all azimuths. A graph analogous to Figure 7 has been drawn but is not reproduced here. The silhouette of surrounding mountains is on the whole below the horizontal and the local sunrise/sunset and radiation totals are again not substantially affected.

Figure 9 displays measurements of SW↓ during all days at the summit site, in the same format as Figure 6. Daily totals, corresponding to the smoothed daily running means representative of completely clear sky and overcast, along with their ratio, are listed in Table II. An estimate of the daily total averaged for 8, 9, and 10 July is also included.

A few particularly large radiation values stand out in Figure 9 and also Figure 6. These measurements were as a rule taken immediately after the sun was cleared from an obstructing cloud. Extreme reflection conditions at cloud base and the high-albedo snow surface seem to be factors for these excessively high spot readings. It is recalled that Untersteiner (1957)
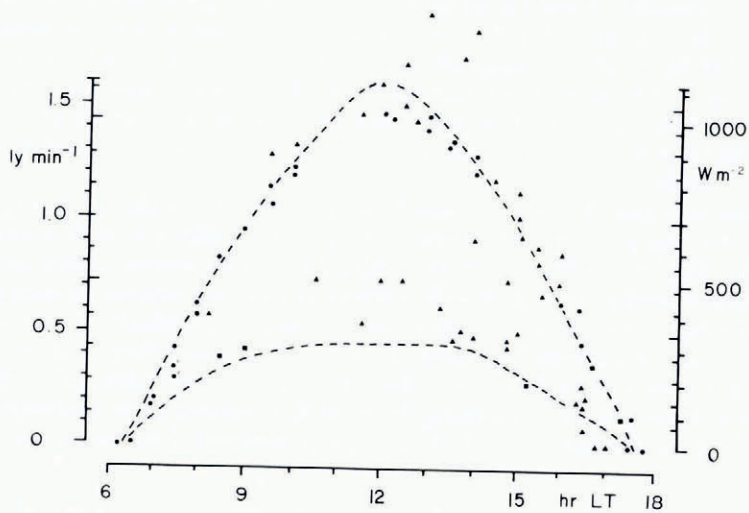
Fig. 9. Global radiation at summit site. Symbols as in Figure 6. Accents identify measurements in fog.

measured instantaneous values as high as 2.6 cal cm^{-2} min^{-1} ($=$ 1 793 W m^{-2}) on Chogo Lungma Glacier in the Karakoram, at high sun, with cloudy sky, and at an elevation of 6 400 m.

Sampling by varying fractions of cloudiness is less satisfactory than for the base-camp site. This should be taken into account in comparing the values in Table II. The daily total of global radiation representative of a completely clear day is somewhat larger for the summit as compared with the base-camp series. This is qualitatively consistent with the higher elevation and the smaller positive solar declination for the summit measurements.

Measurements of LW↑↓ during all nights together are plotted in Figure 10 in a way analogous to Figure 8. Due to the scarcity of sampling at intermediate fractions of cloud cover, differences between Figures 10 and 8 cannot be discussed. However, the decreased net long-wave radiation with increasing cloudiness is also clearly borne out for the summit site. Estimates of LW↑↓ representative of completely clear and overcast sky are given in Table II along with averages for the nights following 7, 8, and 9 July.

Measurements in the immediate vicinity of the summit site and extended traverses across the ice cap (Fig. 1) provided a good spatial and temporal sampling of surface albedo. Use was made of the surveyed accumulation/ablation stakes for accurate location of albedo
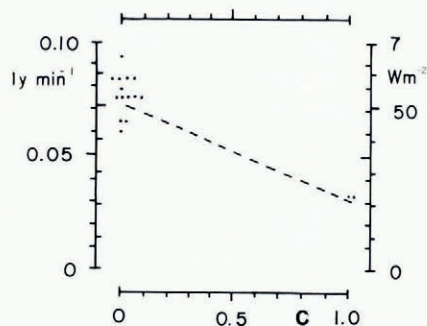

Fig. 10. Night-time net long-wave radiation LW↑↓ at summit site with various cloud cover C.

measurements. Typically, albedo is around 80%, and over parts of the plateau in excess of 90%. Albedo values as low as 40% were measured at lower elevations near the ice rim. Changes from before to after a snowfall are largest in the lower parts of the ice cap but comparatively small over most of the high plateau. The spatial pattern is dominated by an increase of albedo with elevation. It appears appropriate to assign representative albedo values by given elevation bands (Table I). This is useful in later estimates of the radiation budget for the ice cap as a whole.

Some insight into the ablation conditions at the summit site during 7–10 July could be obtained from the "poor man's lysimeters". At no time could any melt water be drained from the bowls. This is consistent with the continuously sub-freezing temperatures. Despite some randomness between the three bowls, a slight weight decrease was generally found from morning to evening, followed by a weight gain of similar magnitude by the next morning. It is noted that these were nights without snowfall. The most substantial overnight weight increase occurred from 9 to 10 July, when dense fog lay over the station. For the period 7–10 July, the typical mass loss from morning to evening is estimated at a water equivalent of 0.1 mm, and the net mass loss over the entire 72 h period at a fraction of that, or essentially nil.

EMPIRICAL FORMULAE

Various empirical formulae have been proposed (Budyko, 1956; Sellers, [c1965]; Cox and Hastenrath, 1970) to calculate radiative fluxes from the more commonly available meteorological elements. Measurements during the 1976 expedition are to be used to estimate coefficients in the empirical equations appropriate for the radiation conditions in the 500 mbar region of the Quelccaya ice cap. This would allow a computation of the radiative flux components representative of the ice plateau as a whole for an entire year, based on the record of conventional meteorological elements expected from our automatic stations.

For the computation of global radiation, Budyko (1956) proposed

$$SW\downarrow = (SW\downarrow)_0(1 - kC) \tag{1}$$

where the subscript 0 refers to a completely cloudless day. Budyko accordingly provided a table of $(SW\downarrow)_0$ values by calendar month and latitude, presumably for sea-level. C signifies total cloudiness and k is an empirical coefficient for which a numerical value of 0.67 is given at lat. 10–15°.

In order to use a relation in the form of Equation (1), values of $(SW\downarrow)_0$ and k representative of Quelccaya are needed. Then daily/monthly totals of $SW\downarrow$ could be calculated from records of sunshine duration, which are to be processed by 1 h periods in local time. $(SW\downarrow)_0$ is available from Figures 6 and 9, and Table II, for the particular solar declinations of $+23°17'$ and $+22°28'$, corresponding to the averages of the measurement days. The respective daily totals at the top of the atmosphere $SW\downarrow_{top}$ based on a solar constant of 1.94 cal cm^{-2} min^{-1} ($= 1 352$ W m^{-2}) are also included in Table II. Extraterrestrial values (List, 1951; Bernhardt and Philipps, 1958) by calendar month and for the latitude of Quelccaya are listed in Table III.

TABLE III. MONTHLY MEANS OF RADIATION $SW\downarrow$ AT QUELCCAYA ICE CAP IN W m^{-2}. "TOP" AND "CLEAR" DENOTE VALUES AT THE TOP OF THE ATMOSPHERE AND GLOBAL RADIATION AT THE SURFACE FOR COMPLETELY CLEAR DAYS, RESPECTIVELY

	J	F	M	A	M	J	J	A	S	O	N	D	Year
Top	463	452	426	380	335	310	319	356	403	339	458	464	401
Clear	454	443	417	372	329	303	313	349	395	430	448	455	393

The ratio of SW↓ at the surface to that at the top of the atmosphere characterizes the transmissivity of the air column over Quelccaya. With half of the atmospheric mass, almost all the moisture, and dust sources, below the level of the ice cap, the optical properties of the atmospheric column are regarded as essentially constant throughout the year. Even so, the ratio $(SW\downarrow)_0/SW\downarrow_{top}$ varies in the course of the year as a result of differing radiation geometry. Sample calculations (Bernhardt and Philipps, 1958) for constant turbidity and the latitude of Quelccaya indicate that the seasonal variation of this ratio stays within a few per cent. Therefore, a constant ratio $(SW\downarrow)_0/SW\downarrow_{top} = 0.98$, as deduced from the 1976 measurements, was used to compute $(SW\downarrow)_0$ from the information in Figures 6, 9, and Table II (see Table III). More sophisticated procedures to compute the ratio $(SW\downarrow)_0/SW\downarrow_{top}$ are available (Shettle and Weinman, 1970) but did not seem warranted for the present purposes. The large ratio of 0.98 at Quelccaya is related to the high elevation and surface albedo, and multiple downward scattering. By way of comparison, Untersteiner's (1958) measurements at 4 300 m in the Karakoram yield a ratio of 0.88.

The ratio of SW↓ for an overcast to that for a completely clear day (Figs 6 and 9; Table II) does not differ significantly between the base-camp and summit sites, if one considers the different sampling of fractional cloud cover. Accordingly, an approximate value of $k = 0.7$ appears acceptable for Quelccaya. It should then be possible to calculate monthly values of SW↓ at actual cloudiness from the expected one-year record of sunshine duration. Although the relationship between daily totals of global radiation and cloudiness is not strictly linear (Untersteiner, 1957), Equation (1) is considered adequate for practical purposes.

The following empirical formula has been proposed for the computation of net long-wave radiation at clear sky (Budyko, 1956; Sellers, [c1965])

$$(LW\uparrow\downarrow)_0 = \epsilon\sigma T^4(0.39 - 0.05\sqrt{e}) \qquad (2)$$

where ϵ signifies emissivity, $\sigma = 826 \times 10^{-13}$ cal cm^{-2} min^{-1} K^{-4} ($= 567 \times 10^{-10}$ W m^{-2} K^{-4}) is the Stefan–Boltzmann constant, e vapor pressure in mbar and T temperature in K.

For the computation of net long-wave radiation at cloudy sky, the following formula has been proposed (Budyko, 1956; Sellers, [c1965]) which also accounts for the effect of thermal stratification near the surface:

$$LW\uparrow\downarrow = (LW\uparrow\downarrow)_0(1 - 0.53C^2) + 4\epsilon\sigma T_0^3(T_0 - T). \qquad (3)$$

Here T_0 is the surface temperature.

Net long-wave radiation at clear sky can also be obtained graphically from the "Integrated Elsasser Chart" (Sellers, [c1965]), instead of Equation (2).

Since temperature and humidity were measured concurrently with LW↑↓, the direct measurements plotted in Figures 8 and 10 can be compared with Equation (2) and the "Integrated Elsasser Chart". Measured values are on the whole about 0.01 cal cm^{-2} min^{-1} ($= 7$ W m^{-2}) smaller than the computed figures. The Quelccaya ice cap has an environment rather unlike the one from which the empirical formula (2) was derived. It is noted, however, from the second right-hand term of Equation (3), that the difference in radiation values could be brought about by a temperature inversion of the order of a few degrees C. In context, the agreement between measured and computed values for clear sky is considered acceptable. Surface inversions are a typical night-time phenomenon, and reliable measurements of LW↑↓ could be made only at night, as discussed on p. 88. Therefore, preference is given to Equation (2) and the graphical procedure (Sellers, [c1965]) for obtaining daily averages of net long-wave radiation at clear sky $(LW\uparrow\downarrow)_0$.

A marked effect of cloudiness on LW↑↓ is apparent from Figures 8 and 10. In view of the restricted sampling of fractional cloud cover, measurements are considered compatible with Equation (3). Accordingly, it is intended to derive monthly mean values of LW↑↓ from Equation (2) or the "Integrated Elsasser Chart", and Equation (3), but without accounting

for the second right-hand term. Temperature and sunshine records from our automatic stations for an entire year will serve as the basic input, with reasonable values adopted for atmospheric humidity, and any systematic day–night differences in cloudiness disregarded.

CONCLUSIONS

A more complete picture of the heat- and mass-budget characteristics of the Quelccaya ice cap is expected from the evaluation of records to be obtained from the automatic stations, and field work envisaged for later years. However, some preliminary inferences can already be made from the June–August 1976 expedition.

The heat-budget equation for the ice surface can, in approximate form, be written

$$\mathrm{SWLW}{\uparrow}{\downarrow} = Q_t - Q_i - Q_s - Q_L + Q_m. \tag{4}$$

All fluxes which transport energy to the surface are considered to be positive, i.e. in the air these fluxes are directed downward, but in the ice they are directed upward. Here $\mathrm{SWLW}{\uparrow}{\downarrow}$ is net radiation; Q_t is heat stored in the ice per unit surface and time; Q_i is conductive heat flux in the ice; Q_s is sensible heat flux; Q_L is latent heat flux; Q_m is heat used in melting per unit surface and time.

The vertical temperature profile at the Quelccaya summit is characterized by a surface temperature of about $-6°\mathrm{C}$ and an increase to around $0°\mathrm{C}$ at 8–10 m depth. This profile is suggestive of surface cooling and heat flux directed from the bedrock upward to the ice surface. Implications of this temperature profile in terms of geothermal heat flux, ice thickness, accumulation rate and surface-heat budget are being studied based on the theory developed by Budd and others (1971). Specifically, the profile suggests that the left-hand and the last three right-hand terms of Equation (4) combine to a net cooling at the surface in the long-term mean. The first two right-hand terms may be understood as representing ice heat loss and geothermal effects. Aside from the latter process, climatic variation would make the first right-hand term different from zero even in the annual mean. To be sure, this term is only a small difference between large terms.

Figures 6 and 8–10, and Table II, provide estimates for the left-hand terms of Equation (4); $\mathrm{SW}{\uparrow}$ is obtained from $\mathrm{SW}{\downarrow}$ and albedo (Tables I and II). For the net radiation $\mathrm{SWLW}{\uparrow}{\downarrow}$, i.e. the sum of the three left-hand terms of Equation (4), the following daily totals are computed from Table II and an albedo of 80% for the summit site: 21, 0 and -4 cal cm^{-2} d^{-1} (approximately 10, 0 and -2 W m^{-2}), for the categories clear sky, overcast, and all days, respectively.

No direct measurements are available for the right-hand terms of Equation (4). The vertical turbulent flux of sensible heat Q_s is related to the temperature difference at the snow–air interface. The latter can become large with marked atmospheric advection, such as during föhn in alpine valleys. In such extreme situations, Q_s may be substantial. For the environment of Quelccaya, however, Q_s is believed to be small compared to other terms of Equation (4). The first right-hand term is also small, as discussed above. Further, melting as an ablation mechanism over most of the plateau is precluded. This is consistent with the sub-freezing temperatures and direct observation. Thus the net radiation $\mathrm{SWLW}{\uparrow}{\downarrow}$ essentially provides the energy for sublimation. The aforementioned daily totals of $\mathrm{SWLW}{\uparrow}{\downarrow}$ correspond to water equivalents of the order of 0.03 mm d^{-1} for clear and much less for cloudy sky. These figures should be compared to the ablation measured in the 72 h average of a fraction of 0.1 mm d^{-1}. Values are well within the error limits of both the residual estimate of $\mathrm{SWLW}{\uparrow}{\downarrow}$ and the ablation measurements.

Albedo in excess of 80% is characteristic of the larger elevated area of the Quelccaya plateau (Fig. 1 and Table I). This leaves for $\mathrm{SW}{\uparrow}{\downarrow}$ a value of the same general magnitude as

$LW\uparrow\downarrow$. Here $SW\uparrow\downarrow$ is directed downward and $LW\uparrow\downarrow$ upward, and the two fluxes approximately cancel. The effect of cloudiness on $SW\downarrow$ and $LW\uparrow\downarrow$ is largely compensatory. Consequently, the energy available for ablation is very small, not only for the period of the expedition but presumably also for the year as a whole. This seemingly delicate balance invites quantitative consideration of geothermal effects and climatic change (e.g. trends in ice temperature).

Over the greater part of the ice cap, ablation may be near to nil, i.e. accumulation approximately equalling net balance. Some ablation, including melting, takes place in the lower-lying marginal strip of the ice body, as is also manifested by subglacial streams and small lakes at the rim of the ice. However, a major mechanism for the disposal of the ice mass, and the potential for ice wastage at lower, warmer locations, with smaller albedo, seems to be provided by spectacular calving of steep cliffs.

REFERENCES

Bernhardt, F., *and* Philipps, H. 1958. Die räumliche und zeitliche Verteilung der Einstrahlung, der Ausstrahlung und der Strahlungsbilanz im Meeresniveau. Teil 1. Die Einstrahlung. *Abhandlungen des Meteorologischen und Hydrologischen Dienstes der Deutschen Demokratischen Republik*, Nr. 45.

Budd, W. F., *and others.* 1971. Derived physical characteristics of the Antarctic ice sheet, by W. F. Budd, D. Jenssen and U. Radok. *ANARE Interim Reports.* Ser. A (IV). Glaciology. Publication No. 120.

Budyko, M. I. 1956. *Teplovy balans zemnoy poverkhnosty* [*The heat balance of the Earth's surface*]. Leningrad, Gidrometeorologicheskoye Izdatel'stvo. [English translation published by U.S. Weather Bureau, Washington, D.C., 1958.]

Cox, S. K., *and* Hastenrath, S. 1970. Radiation measurements over the equatorial central Pacific. *Monthly Weather Review*, Vol. 98, No. 11, p. 823–32.

List, R. J. 1951. Smithsonian meteorological tables. Sixth revised edition. *Smithsonian Miscellaneous Collections*, Vol. 114. (Publication 4014.)

Mercer, J. H., *and others.* 1975. Peru's Quelccaya ice cap: glaciological and glacial geological studies, 1974, [by] J. H. Mercer and L. G. Thompson, C. Marangunič, J. Ricker. *Antarctic Journal of the United States*, Vol. 10, No. 1, p. 19–24.

Peru. Ministerio de Agricultura. Oficina de Catastro Rural. 1976. Cuzco, hoja 28 u–III–SE. Lima, Oficina de Catastro Rural. [Map, 1 : 25 000.]

Sellers, W. D. [c1965]. *Physical climatology.* Chicago and London, University of Chicago Press.

Shettle, E. P., *and* Weinman, J. A. 1970. The transfer of solar irradiance through inhomogeneous turbid atmospheres evaluated by Eddington's approximation. *Journal of the Atmospheric Sciences*, Vol. 27, No. 7, p. 1048–55.

Untersteiner, N. 1957. Glazial-meteorologische Untersuchungen im Karakorum. I. Strahlung. *Archiv für Meteorologie, Geophysik und Bioklimatologie*, Ser. B, Bd. 8, Ht. 1, p. 1–30.

4